Journal of Materials Chemistry

Dynamic Article Links

Cite this: *J. Mater. Chem.*, 2011, **21**, 6088

www.rsc.org/materials

PAPER

Fabrication of pyrenetetrasulfonate/layered double hydroxide ultrathin films and their application in fluorescence chemosensors†

Wenying Shi, Yanjun Lin, Xianggui Kong, Shitong Zhang, Yankun Jia, Min Wei,* David G. Evans and Xue Duan

Received 6th January 2011, Accepted 24th February 2011
DOI: 10.1039/c1jm00073j

This paper reports the fabrication of fluorescence indicator/layered double hydroxide (LDH) ultrathin films (UTFs) by alternate assembly of 1,3,6,8-pyrenetetrasulfonat acid tetrasodium salt (PTS) and Zn–Al LDH nanosheets on quartz substrates using the layer-by-layer (LBL) deposition technique, and demonstrates their application as a fluorescence chemosensor for Cu^{2+}. UV-vis absorption spectroscopy indicates a stepwise and regular growth of the PTS/LDH UTFs upon increasing deposition cycles. X-Ray diffraction, atomic force microscopy and scanning electron microscopy demonstrate that the UTFs possess a periodical layered structure perpendicular to the substrates with a thickness of 1.93–1.98 nm per bilayer. Furthermore, the fluorescence chemosensor with film thickness of 48 nm (24 bilayers) exhibits a broad linear response range for Cu^{2+} solution (0.6–50 μM), good repeatability (RSD less than 5% in 20 consecutive measurements), high photostability and storage stability (~93.2% of its initial fluorescence intensity remains after one month) as well as excellent selectivity. In addition, the study on mechanism of measurement-regeneration cycle of the fluorescence chemosensor shows that Cu^{2+} enters/departs from the PTS/LDH UTF with reversible change in chemical composition, surface morphology and fluorescence anisotropy. Therefore, this work provides new opportunities for fabrication and application of chromophore/LDH UTFs which can be used as fluorescence chemosensors.

1. Introduction

The development of sensors based on artificial receptors for the detection of environmentally and biologically important species, such as heavy-metal ions, has received considerable attention in the past few years.[1] A chemosensor is defined as a molecule of abiotic origin that reversibly cooperates with an analyte accompanied by a signal transduction.[2] The fluorescence chemosensors are envisioned as one of the most promising candidates for the development of innovative sensing systems in many different kinds of sensors, due to their sensitivity, specificity and real-time monitoring with fast response.[3]

Copper is a significant metal pollutant due to its widespread usage, but it is also a micronutrient element in biological systems.[4] Copper has multiple functions ranging from iron absorption and reduction–oxidation to catalysis.[5] However, copper can cause oxidative stress and disorders associated with neurodegenerative diseases if being unregulated, such as Menkes disease, Wilson disease and Alzheimer's disease.[6] Recently, a great number of fluorescence chemosensors for copper ions have been successfully designed due to their high selectivity and sensitivity.[7] Especially, the organic-fluorescence film chemosensors have realized repetitive utilization without consumption or contamination to the analyte solution.[8] However, organic films usually suffer from long-term sustainability as the result of variation in illumination, temperature, pressure, environmental pH, *etc.* Therefore, the incorporation of organic fluorophore indicator with inorganic matrix can be an effective solution for the purpose of obtaining durable solid chemosensors.

Layered double hydroxides (LDHs), whose structure can be generally expressed as $[M^{II}_{1-x}M^{III}_{x}(OH)_2](A^{n-})_{x/n}\cdot mH_2O$ (M^{II} and M^{III} are divalent and trivalent metals respectively; A^{n-} a *n*-valent anion), are one type of important layered materials which represent a large versatility in terms of their chemical composition and the ability to build up 2D-organized structures (stacking of the layers giving rise to an accessible interlayer space in the nanometre scale).

State Key Laboratory of Chemical Resource Engineering, Beijing University of Chemical Technology, Beijing, 100029, China. E-mail: weimin@mail.buct.edu.cn; Fax: +86-10-64425385; Tel: +86-10-64412131

† Electronic supplementary information (ESI) available: The UV-vis absorption and emission spectra (Figure S1); SEM side views (Figure S2); SEM image (Figure S3); AFM image (Figure S4); Schematic representation of assembly and structure (Figure S5); Response time and correlation between the response time and *n* (Figure S6); SEM image (Figure S7) and fluorescence decay data (Table S1). This material is available free of charge *via* the internet at http://rsc.calis.edu.cn/main/journalscan.asp. See DOI: 10.1039/c1jm00073j

They are available as both naturally occurring minerals and synthetic inorganic materials,[9] which have been widely used in the fields of catalysis, separation process, biology and medicine.[10] Some sensors based on LDH and fluorophore composites have also been successfully developed normally *via* the dip-coating,[11] electrophoretic deposition[12] and solvent evaporation method.[13] Recently, the delamination of LDH into nanosheets as building blocks and preparation of inorganic/organic fluorophore ultrathin films (UTFs) have been reported.[14] This inspired us to challenge the goal of fabricating fluorescent chemosensors *via* alternate assembly of positively charged LDH nanosheets and negatively charged fluorophore indicators with the layer-by-layer (LBL) technique, which exhibit the following advantages: the LDH nanosheets provide a confined and stable microenvironment for the immobilization of fluorophore indicator; the nanometre scale control of the assembly will result in a high dispersion of fluorophore with uniform orientation, suppressing chromophore aggregation and reducing fluorescence quenching. Moreover, the film component and thickness can be precisely controlled with simple manipulation and versatility.

Pyrene and its derivatives have been widely used in the fields of organic light-emitting devices,[15] field-effect transistors,[16] liquid crystals,[17] biological markers,[18] ion sensors[19] and conformational probes due to their high detection sensibility.[20] However, the application of pyrene and its derivatives is greatly limited owing to the relatively short service lifetime, unsatisfactory stability and fluorescence quenching resulted from aggregation. Therefore, how to improve their luminescence performances remains a challenge. In this work, fluorescence indicator/LDH UTFs were fabricated by alternate assembly of 1,3,6,8-pyrenetetrasulfonate acid tetrasodium salt (PTS) and Zn–Al LDH nanosheets on quartz substrates using the LBL deposition technique, which was successfully demonstrated as fluorescence chemosensor for Cu^{2+}. The fluorescence chemosensor with film thickness of 48 nm (24 bilayers) exhibits a broad linear response range for Cu^{2+} solution (0.6–50 μM), good repeatability (RSD less than 5% in 20 consecutive measurements), high photostability and storage stability (~93.2% of its initial fluorescence intensity remains after one month) as well as excellent selectivity. Therefore, the novel strategy in this work provides a facile approach for the fabrication of luminescence film with nanoscale control of thickness, which can be potentially applied in the field of optical sensors.

2. Experimental

2.1 Materials

1,3,6,8-Pyrenetetrasulfonic acid tetrasodium salt (PTS, biochemistry grade) was purchased from Sigma-Aldrich Company. Analytical grade chemicals including Zn $(NO_3)_2 \cdot 6H_2O$, $Al(NO_3)_3 \cdot 9H_2O$, NaOH, C_2H_5OH, $Cu(NO_3)_2$, $Co(NO_3)_2$, $Ni(NO_3)_2$, $Pb(NO_3)_2$ and ethylenediamine tetraacetic acid (EDTA) were used without further purification. The deionized and decarbonated water was used in all the experimental processes.

2.2 Fabrication of the $(PTS/LDH)_n$ UTFs

The $Zn_2Al\text{-}NO_3$ LDH precursor was synthesized by the hydrothermal method reported previously.[21] A 0.1 g of Zn–Al-LDH was shaken in 100 mL of formamide solution for 24 h to obtain a colloidal suspension of exfoliated Zn–Al-LDH nanosheets. The quartz glass substrate was cleaned in concentrated NH_3/30% H_2O_2 (7 : 3) and concentrated H_2SO_4 for 30 min each. After each procedure, the quartz substrate was rinsed and washed thoroughly with deionized water. The substrate was dipped in a colloidal suspension (0.1 g mL^{-1}) of LDH nanosheets for 10 min followed by washing thoroughly, and then the substrate was treated with a 100 mL of PTS aqueous solution (0.025 wt%) for another 10 min followed by washing. Multilayer films of $(PTS/LDH)_n$ were fabricated by alternate deposition of LDH nanosheets suspension and PTS solution for n cycles. The resulting films were dried with a nitrogen gas flow for 2 min at 25 °C.

2.3 The response of Cu^{2+} measurement

The Cu^{2+} solutions with different concentrations were prepared by dissolving $Cu(NO_3)_2$ in a water–ethanol mixture solvent (1 : 1, v/v, 295 K). The fluorescence chemosensor was immersed into a quartz cell with $Cu(NO_3)_2$ solution, and its response was recorded by a RF-5301PC fluorophotometer with a liquid holder. Between two different concentration measurements the chemosensor was washed thoroughly with deionized and decarbonated water.

2.4 Characterization techniques

The UV-vis absorption spectra were collected in the range from 200 to 500 nm on a Shimadzu T-9201 spectrophotometer, with the slit width of 1.0 nm. The fluorescence spectra were performed on a RF-5301PC fluorospectrophotometer with the excitation wavelength of 340 nm. The fluorescence emission spectra range in 350–550 nm, and both the excitation and emission slits were set to 3 nm. The fluorescence image was observed using an OLYMPUS-BX51 fluorescence microscope. The photobleaching behavior was tested by the UV lighting with CHF-XQ 500 W. Steady-state polarized photoluminescence measurements of the PTS/LDH UTFs were recorded with an Edinburgh Instruments' FLS 920 fluorospectrophotometer. X-Ray diffraction patterns (XRD) of the PTS/LDH UTFs were recorded using a Rigaku 2500 VB2 + PC diffractometer under the conditions: 40 kV, 50 mA, Cu-Kα radiation (λ = 0.154056 nm) step-scanned with a scanning rate of 2°/min, and a 2θ angle ranging from 2° to 65°. The Fourier transform infrared (FTIR) spectra were recorded using a Vector 22 (Bruker) spectrophotometer in the range 4000–400 cm^{-1} with 4 cm^{-1} resolution. The morphology of thin films was investigated by using a scanning electron microscope (SEM ZEISS) equipped with an EDX attachment, and the accelerating voltage applied was 20 kV. The surface roughness and thickness data were obtained by using the atomic force microscopy (AFM) software (Digital Instruments, version 6.12). X-Ray photoelectron spectroscopy (XPS) measurement was performed with monochromatized A1-Kα exciting X-radiation (PHI Quantera SXM).

3. Results and discussion

3.1 Assembly of the PTS/LDH UTFs

Fig. 1A shows the UV-vis absorption spectra of the $(PTS/LDH)_n$ UTFs with various bilayer numbers (n) deposited on quartz

substrates. It was observed that the absorption bands of pyrene at ~250, 290 and 380 nm (π–π* transition of PTS) correlate linearly with n (Fig. 1B), indicating a stepwise and regular film growth procedure, which was further confirmed by the gradual color enhancement with the increase of bilayer number (inset in Fig. 1A). The value of absorbance is above zero as $n = 0$ observed from the linear regression curve (Fig. 1B), which can be attributed to the decrease in film uniformity and homogeneity during the LBL deposition process. Compared with the absorption spectrum of PTS solution sample (Fig. S1-A†), the absorption band of the $(PTS/LDH)_n$ UTFs becomes broader and unresolved, which may be attributed to the electrostatic interaction between PTS molecule and LDH nanosheets. The fluorescence emission peaks at 375 and 394 nm of $(PTS/LDH)_n$ UTFs also display a consistent increase along with n, as shown in Fig. S1-B†. No obvious red or blue shift of the fluorescence spectra for the as-prepared UTFs was observed compared with the pristine PTS solution, indicating no formation of PTS aggregates throughout the whole assembly process. The fluorescence lifetime of the $(PTS/LDH)_n$ UTFs ranges from 113.5 to 128.6 ns (Table S1 in the ESI†), much longer than that of the pristine PTS solution (80.2 ns). The results above indicate that the rigid LDH nanosheets isolate PTS molecule from each other and thus eliminate the interlayer π–π stacking interaction.

3.2 Structural and morphological characterization

The deposition process of the $(PTS/LDH)_n$ UTFs was further monitored by scanning electron microscopy (Fig. S2-A†). The thickness of the as-prepared UTFs ($n = 10$–40) are in the range of 25–83 nm. The approximately linear increase of the thickness upon increasing the layer number confirms that the UTFs present uniform and periodic layered structure (Fig. S2-B†), in agreement with the behavior revealed by the absorption and fluorescence spectra above. The SEM images (Fig. 2A and Fig. S3†) show that the surface smoothness and uniformity of the UTFs decrease with the increase of bilayer number. The thickness of $(PTS/LDH)_{20}$ UTF is 39 nm observed from its side view of the SEM image (Fig. 2B), from which it can be estimated that the thickness of one bilayer $(PTS/LDH)_1$ is ~1.95 nm. The AFM topographical images (Fig. 2C and Fig. S4†) show the value of root-mean square roughness (RSM) increases from 2.75 nm ($n =$ 5) to 11.7 nm ($n = 20$), indicating the decrease in uniformity of the UTFs along with the assembly of LBL film. XRD patterns (Fig. 2D) exhibit a Bragg peak at $2\theta = 4.25°$ and its intensity increases successively upon increasing n, which can be attributed to a superlattice structure in the normal direction of the film. The average repeating distance is ~1.98 nm, approximately consistent with the thickness augment per deposited cycle observed by SEM (1.95 nm). Moreover, this is also in agreement with the ideal single-layered arrangement model of the PTS/LDH supramolecular structure with the thickness of ~0.48 nm for a monolayer of LDH and 1.45 nm for the extended chain configuration of PTS (Fig. S5†).

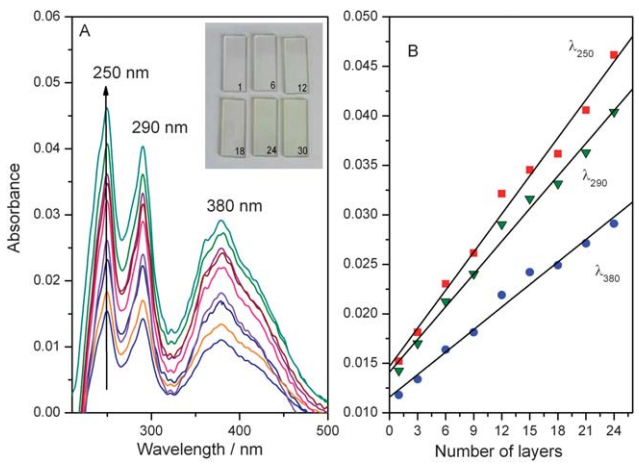

Fig. 1 (A) UV-vis absorption spectra of the $(PTS/LDH)_n$ (n = 1–24) UTFs (inset: the photographs of UTFs with different bilayer numbers under daylight); (B) The linear relationship between absorbance at 250, 290, 380 nm and bilayer number n.

3.3 The $(PTS/LDH)_n$ UTFs as fluorescence chemosensors for Cu^{2+}

The response of $(PTS/LDH)_n$ UTFs for Cu^{2+}. The $(PTS/LDH)_n$ (n=1 − 40) UTFs were fabricated to test its feasibility for Cu^{2+} sensor. Fig. S1-B† and Fig. S6† show the fluorescence spectra and response time of the UTFs with different n (6–36), respectively. It was found that both fluorescence intensity and response time increased upon increasing n. The enhancement in fluorescence intensity results from the increase of PTS content; while the increase in response time is related to the reduced diffusion rate of Cu^{2+} in the film with larger thickness. Taking into account both the fluorescence intensity and response time, the PTS/LDH (48 nm, $n = 24$) UTF sample was chosen in the following study. The response time was 10 s for the $(PTS/LDH)_{24}$ UTF (Fig. S6-B†), which is a key feature for its practical application. Longer response time (from 2 min to 18 h) was generally reported for fluorescence chemosensors based on organic matrices.[8c,8e] The fast response in this work is possibly related to the nanoscale architecture of the PTS/LDH UTF (Fig. 2A), which is preferable for the mass transfer and diffusion.

Fig. 3A displays that the fluorescence intensity of the $(PTS/LDH)_{24}$ UTF decreases with the increase of Cu^{2+} concentration from 0.2 μM up to 1000 μM. The titration plots of this UTF

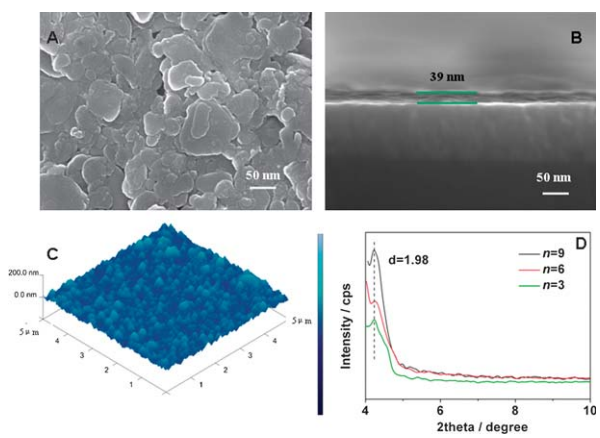

Fig. 2 (A) Top-view of SEM image, (B) side-view of SEM image, (C) tapping-mode AFM image of the $(PTS/LDH)_{20}$ UTF and (D) XRD patterns for the $(PTS/LDH)_n$ UTFs with $n = 3$, 6 and 9 respectively.

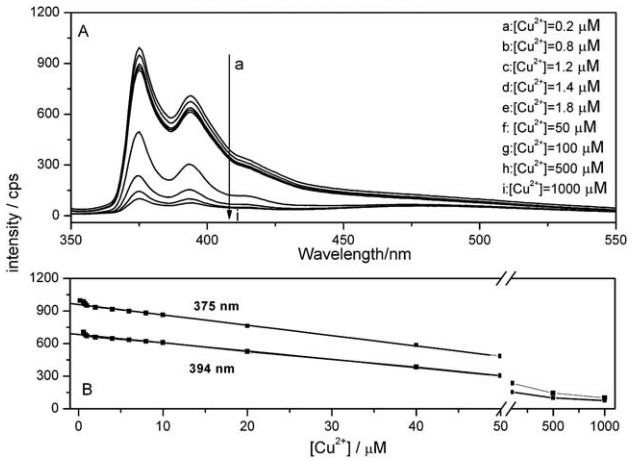

Fig. 3 (A) Emission spectra of the chemosensor with the presence of different Cu^{2+} concentration (295 K, $\lambda_{ex} = 340$ nm); (B) Cu^{2+} titration curves of the chemosensor for emissions at 375 and 394 nm respectively.

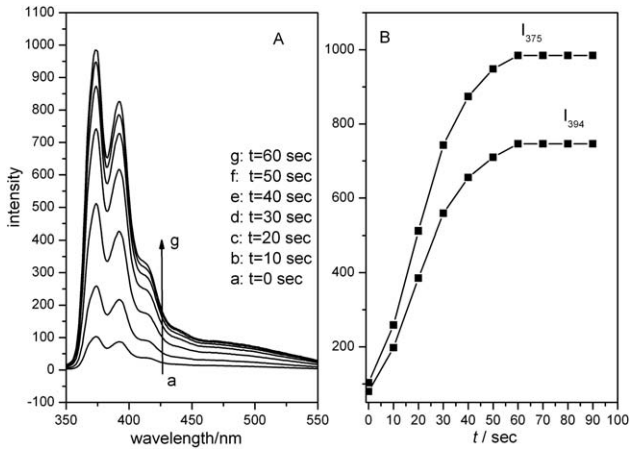

Fig. 4 (A) Emission spectra of the quenched chemosensor in EDTA (0.5 mM, 295 K) as a function of time; (B) The fluorescence intensity at 375 and 394 nm *vs.* *t*.

obtained with excitation of 340 nm and emissions of 375 and 394 nm are displayed in Fig. 3B. The results show that the fluorescence intensity was proportional to the Cu^{2+} concentration in the range 0.6–50 μM, with the following linear regression equation: $I = 959.67–9.48c$ (μM), $r^2 = 0.998$ (Fig. 3B). The absolute detection limit was 0.2 μM, which is sufficient for the determination of Cu^{2+} in the blood system of human (15.7–23.6 μM). Moreover, it meets the requirement for Cu^{2+} detection in drinking water within U.S. EPA limit (~20 μM).[22] The reason for fluorescence quenching of the UTF with the presence of Cu^{2+} is probably due to the occurrence of either an electron transfer or an electronic energy transfer involving the transition metal and the excited fluorophore as observed in other Cu^{2+}-recognition sensors.[23]

The regeneration and reversibility. The regeneration of fluorescence chemosensor was performed by immersing the quenched $(PTS/LDH)_{24}$ UTF into a solution of EDTA (a metal ion chelator, 0.5 mM). Fig. 4A shows that the fluorescence intensity at 375 and 394 nm of the UTF increased gradually and recovered completely after 60 s (Fig. 4B), demonstrating the binding between PTS and Cu^{2+} is chemically reversible. This is a key factor for the preparation of sensor devices in practical application. The repeatability of the chemosensor was studied by alternate immersion into two solutions with Cu^{2+} and EDTA respectively, and the corresponding fluorescence intensity at 375 nm was measured every 2 min (Fig. 5). The RSD of 20 cycles was 4.53% (EDTA) and 1.54% (Cu^{2+}). Additionally, the change of luminescence color (between dark blue and white blue) for the UTF is also reversible by observing its fluorescence microscope image (Fig. 5, inset). Therefore, the regeneration and reversibility of the UTF create new opportunities for the design and application of PTS/LDH UTFs in optical chemosensors.

Stability. The photostability of chemosensor is of major importance, since it leads to irreversible loss of fluorescence, which limits the statistical accuracy of the detection in biological, environmental and physiological applications.[24] The fluorescence intensity of PTS in solution and the $(PTS/LDH)_{24}$ UTF was recorded by illuminating with UV light for comparison study. Fig. 6A displays the fluorescence intensity of these samples as a function of bleaching time. It was found that the half-life of the $(PTS/LDH)_{24}$ UTF sample (6 h) is two times longer than that of the PTS solution (2.5 h), indicating that the rigid LDH nanosheets improve the photostability of PTS molecule significantly. PTS molecules were distributed uniformly and orderly, suppressing the fluorescence quenching effectively. Furthermore, the storage stability test of the sensor shows that ~93.2% of its initial fluorescence intensity remained after one month measurement (Fig. 6B). In addition, as shown in Fig. S7†, no delamination or peeling occurred on cross-cutting the surface, indicating strong adhesion of the film to the substrate. Chemosensors of organic polymer film generally suffer from repeatability, owing to relatively poor thermal or optical stability as well as swelling solution-dependent behavior.[8b,8e] In contrast, the chemosensor of PTS/LDH possesses strong photostability, storage and mechanical stability due to the presence of inorganic component.

Selectivity. An important feature of the chemosensor is its high selectivity toward analyte over other competitive species. In

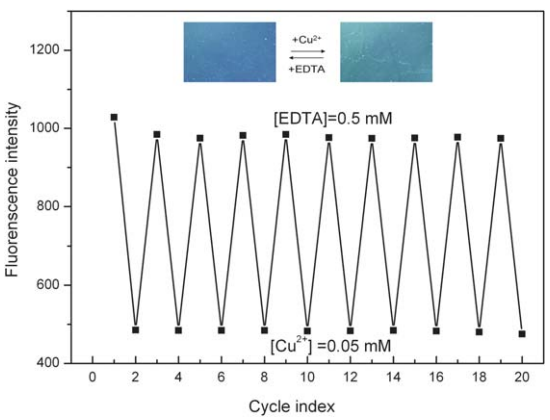

Fig. 5 The reversibility of the chemosensor recorded by alternate measurement in the two solutions of Cu^{2+} and EDTA respectively. The fluorescence microscope images of the chemosensor (inset) show the change of film color.

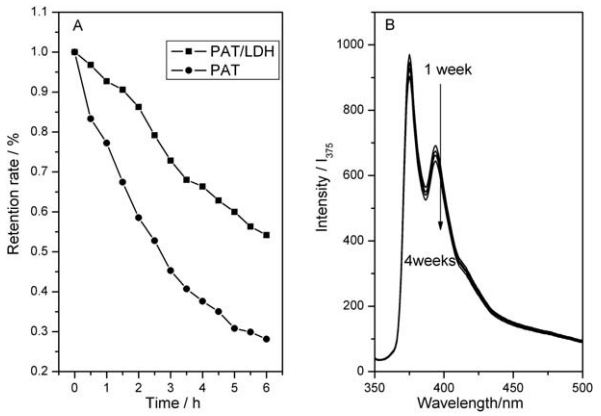

Fig. 6 (A) The photostability of the chemosensor and PTS solution as a function of bleaching time. Indicated values are means of three experiments with the standard error less than 4%. (B) The fluorescence emission spectra of the $(PTS/LDH)_{24}$ UTF (stored at 4 °C) recorded weekly in 1 month.

order to evaluate the selectivity of the $(PTS/LDH)_{24}$ UTF towards Cu^{2+}, the fluorescence intensity at 375 nm for the UTF in solutions containing Co^{2+}, Ni^{2+}, Cu^{2+}, Pb^{2+} and Zn^{2+} was recorded, respectively (Fig. 7A). It was found that the response of the UTF to other cations was very low compared with Cu^{2+}, and less change in the fluorescence intensity of UTF for these interferential species (~10%) than Cu^{2+} (~90%) with the concentration of 1 mM was observed. Moreover, no significant effect on the response of the UTF to Cu^{2+} was found with the presence of Co^{2+}, Ni^{2+}, Pb^{2+} and Zn^{2+} (1 mM each). The fluorescence intensity was still proportional to the Cu^{2+} concentration in the range 0.6–50 μM with $r^2 = 0.991$ (Fig. 7B). The results above show that the UTF exhibits a high selectivity for Cu^{2+}.

3.4 Studies on the mechanism of measurement-regeneration cycle

The change of chemical composition. The process of fluorescence quenching and regeneration for the fluorescence chemosensor is schematically shown in Scheme 1. The fluorescence quenching results from the complexation of Cu^{2+} and PTS in the UTF due to a high thermodynamic affinity of Cu^{2+} for typical O-chelate ligands and fast metal-to-ligand binding kinetics; while the regeneration of the quenched UTF was rooted in the complexation of Cu^{2+} and EDTA due to the much larger complex constant between EDTA and Cu^{2+} ($\log K \approx 9$)[25] than pyrene and Cu^{2+} ($\log K \approx 5$).[26] The explanation was further supported by the results from XPS measurement shown in Fig. 8. Compared with the original UTF (Fig. 8A), the XPS spectrum after measurement of Cu^{2+} (Fig. 8B) displays signals of Cu 2p1/2 (953.5 eV) and Cu 2p3/2 (932.1 eV), indicating that Cu^{2+} was bonded in the UTF *via* the complexation with PTS. The disappearance of Cu signals for the regenerated UTF by EDTA confirms the removal of Cu^{2+} from the UTF (Fig. 8C). In addition, it is known that static quenching is characterized by a constant fluorescence lifetime (τ) of the fluorescence indicator, which is independent of the quencher concentration.[27] In this work, the fluorescence lifetime measurements demonstrated that introduction of Cu^{2+} imposed little effect on the fluorescence lifetime of PTS ($\tau_{treated} = 127.3$ ns, $\tau_{untreated} = 128.6$ ns, Table S1†). Therefore, the fluorescence quenching of the UTF by Cu^{2+} should be static in nature.

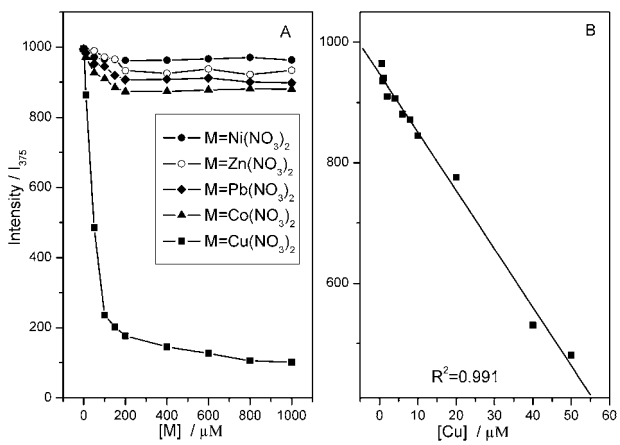

Fig. 7 The spectrofluorimetric titrations of the chemosensor with (A) different metal cations and (B) Cu^{2+} with the presence of interferential species Ni^{2+}, Zn^{2+}, Pb^{2+}, Co^{2+} (1 mM each). Indicated values are means of three measurements with the standard error less than 3%.

The changes in morphology and fluorescence anisotropy. Fig. 9 shows the AFM images of the $(PTS/LDH)_{24}$ UTF during a complete measurement-regeneration process. The original UTF surface (Fig. 9A) is smooth with a large number of round protuberances and a root-mean square roughness of 11.7 nm; while sharp peaks were observed after measurement of Cu^{2+} (Fig. 9B) accompanied with a marked increase in RMS roughness (18.6 nm). After regeneration by EDTA, a relatively smooth surface was recovered with a RMS roughness of 13.3 nm (Fig. 9C). In order to give a further insight for the mechanism of measurement-regeneration cycle, the polarized photoemission spectra of the original $(PTS/LDH)_{24}$ UTF, the quenched and recovered UTF samples were measured and displayed in Fig. 10A–10C, respectively. The original $(PTS/LDH)_{24}$ UTF shows well-defined fluorescence anisotropy between the parallel and perpendicular to excitation polarized direction with the anisotropy value (r) of 0.26 (Fig. 10A) due to well-oriented and ordered arrangement of PTS. However, the anisotropy value decreased dramatically to 0.12 after measurement of Cu^{2+} (Fig. 10B), indicating the decrease in the conjugacy of PTS. After regeneration by EDTA, the fluorescence anisotropy value increased to 0.23 (Fig. 10C) owing to the removal of Cu^{2+} from

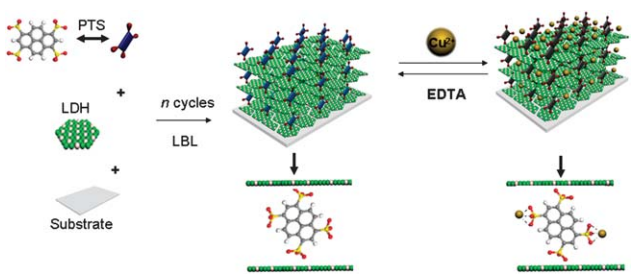

Scheme 1 The schematic representation for the measurement-regeneration cycle of the UTF.

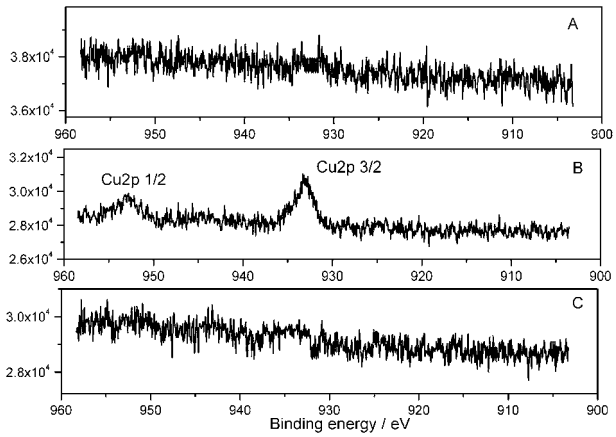

Fig. 8 XPS spectra of (A) the original UTF, (B) the UTF after measurement of Cu^{2+}, (C) the regenerated UTF by EDTA.

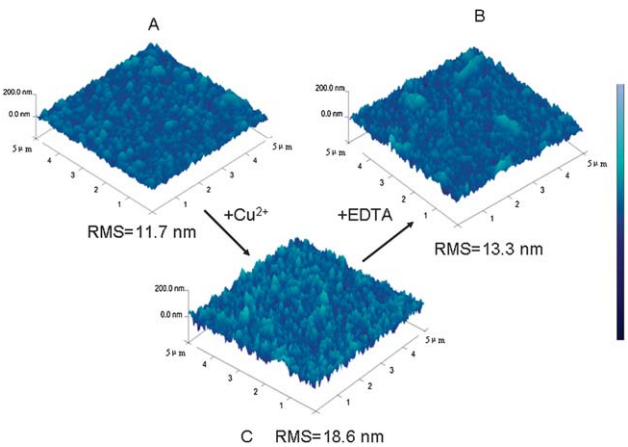

Fig. 9 AFM images of (A) the original $(PTS/LDH)_{24}$ UTF, (B) the UTF after measurement of Cu^{2+}, (C) the regenerated UTF by EDTA.

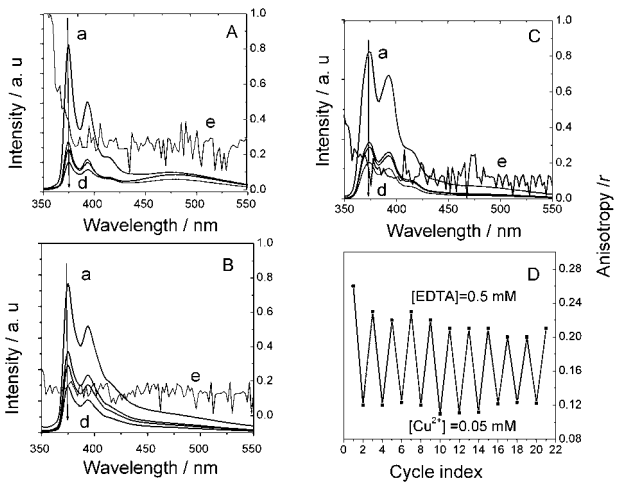

Fig. 10 Photoemission profiles in the (a) VV, (b) VH, (c) HV, (d) HH, (e) polarizations and anisotropy of the sample measured at room temperature (293 K): (A) the original $(PTS/LDH)_{24}$ UTF, (B) the UTF after measurement of Cu^{2+}, (C) the regenerated UTF by EDTA and (D) the fluorescence anisotropy over 20 cycles. The excitation wavelength is 340 nm.

the UTF. The reversible change in anisotropy can also be recycled (Fig. 10D) and the RSD of 20 cycles was 1.71% (EDTA) and 0.52% (Cu^{2+}), indicating that the embedment/removal of Cu^{2+} gives rise to regular changes in orientation of PTS.

4. Conclusions

The ordered $(PTS/LDH)_n$ UTFs were fabricated by the LBL deposition technique in this work, which exhibit application as a fluorescence chemosensor for Cu^{2+}. The UV-vis absorption and the fluorescence emission spectra show a stepwise and regular film growth procedure. The rigid LDH nanosheets isolate PTS molecules from each other and thus eliminate the interlayer π–π stacking interaction. Furthermore, the $(PTS/LDH)_{24}$ UTF as fluorescence chemosensor for Cu^{2+} was obtained, which shows a broad linear response range, good regeneration and reversibility, high photostability, storage and mechanical stability as well as selectivity. The mechanism study of the measurement-regeneration cycle reveals that the embedment/removal of Cu^{2+} gives rise to regular changes in chemical composition, surface morphology and fluorescence anisotropy of the UTF. Therefore, this work provides a facile and feasible methodology for the fabrication of novel fluorescence chemosensors. By virtue of the highly tunable compositions both for inorganic and for organic parts, these multilayer films can be potentially applied in the fields of optical coatings, photosensors and photovoltaic devices.

Acknowledgements

This project was supported by the 973 Program (Grant No. 2011CBA00504), the National Natural Science Foundation of China, the 111 Project (Grant No. B07004) and the Postdoctoral Science Foundation (Grant No. 20100480183).

Notes and references

1 (*a*) A. P. de Silva, H. Q. N. Gunaratne, T. Gunnlaugsson, A. J. M. Huxley, C. P. McCoy, J. T. Rademacher and T. E. Rice, *Chem. Rev.*, 1997, **97**, 1515; (*b*) E. M. Nolan and S. J. Lippard, *J. Mater. Chem.*, 2005, **15**, 2778; (*c*) T. Gunnlaugsson, T. C. Lee and R. Parkesh, *Org. Lett.*, 2003, **5**, 4065.
2 (*a*) T. W. Bell and N. M. Hext, *Chem. Soc. Rev.*, 2004, **33**, 589; (*b*) G. Qian, X. Li and Z. Y. Wang, *J. Mater. Chem.*, 2009, **19**, 522.
3 (*a*) J. S. Kim and D. T. Quang, *Chem. Rev.*, 2007, **107**, 3780; (*b*) E. Rampazzo, E. Brasola, S. Marcuz, F. Mancin, P. Tecilla and U. Tonellato, *J. Mater. Chem.*, 2005, **15**, 2687; (*c*) N. B. Sankaran, S. Nishizawa, M. Watanabe and T. Uchida, *J. Mater. Chem.*, 2005, **15**, 2755; (*d*) M. Montalti, L. Prodi and N. Zaccheroni, *J. Mater. Chem.*, 2005, **15**, 2810; (*e*) D. W. Domaille, L. Zeng and C. J. Chang, *J. Am. Chem. Soc.*, 2010, **132**, 1194.
4 L. Mei, Y. Xiang, N. Li and A. Tong, *Talanta*, 2007, **72**, 1717.
5 D. W. Domaille, E. L. Que and C. J. Chang, *Nat. Chem. Biol.*, 2008, **4**, 168.
6 K. J. Barnham, C. L. Masters and A. I. Bush, *Nat. Rev. Drug Discovery*, 2004, **3**, 205.
7 (*a*) X. He, H. Liu, Y. Li, S. Wang, Y. Li, N. Wang, J. Xiao, X. Xu and D. Zhu, *Adv. Mater.*, 2005, **17**, 2811; (*b*) H. S. Jung, P. S. Kwon, J. W. Lee, J. Kim, C. S. Hong, J. W. Kim, S. Yan, J. Y. Lee, J. H. Lee, T. Joo and J. S. Kim, *J. Am. Chem. Soc.*, 2009, **131**, 2008; (*c*) J. F. Zhang, Y. Z. J. Yoon, Y. Kim, S. J. Kim and J. S. Kim, *Org. Lett.*, 2010, **12**, 3852.
8 (*a*) Y. J. Zheng, K. M. G. Asfura, V. Konka and R. M. Leblanc, *Chem. Commun.*, 2002, 2350; (*b*) A. Torrado, G. K. Walkup and B. Imperiali, *J. Am. Chem. Soc.*, 1998, **120**, 609; (*c*) R. Krämer, *Angew. Chem., Int. Ed.*, 1998, **37**, 772; (*d*) M. Beltramello, M. Gatos, F. Mancin, P. Tecilla and U. Tonellato, *Tetrahedron*

Lett., 2001, **42**, 9143; (*e*) Y. Zhang, K. M. G. Asfura, C. Li, F. M. Andreopoulos, S. M. Pham and R. M. Leblanc, *J. Phys. Chem. B*, 2003, **107**, 483; (*f*) Y. Zheng, J. Orbulescu, X. Ji, F. M. Andreopoulos, S. M. Pham and R. M. Leblanc, *J. Am. Chem. Soc.*, 2003, **125**, 2680.

9 (*a*) A. I. Khan, L. X. Lei, A. J. Norquist and D. O'Hare, *Chem. Commun.*, 2001, 2342; (*b*) J. A. Gursky, S. D. Blough, C. Luna, C. Gomez, A. N. Luevano and E. A. Gardner, *J. Am. Chem. Soc.*, 2006, **128**, 8376; (*c*) A. M. Fogg, A. J. Freij and G. M. Parkinson, *Chem. Mater.*, 2002, **14**, 232.

10 (*a*) A. M. Fogg, V. M. Green, H. G. Harvey and D. O'Hare, *Adv. Mater.*, 1999, **11**, 1466; (*b*) A. M. Fogg, J. S. Dunn, S. G. Shyu, D. R. Cary and D. O'Hare, *Chem. Mater.*, 1998, **10**, 351; (*c*) J. H. Choy, S. Y. Kwak, J. S. Park, Y. J. Jeong and J. Portier, *J. Am. Chem. Soc.*, 1999, **121**, 1399.

11 E. Han, D. Shan, H. Xue and S. Cosnier, *Biomacromolecules*, 2007, **8**, 971.

12 (*a*) T. W. Kim, M. Sahimi and T. T. Tsotsis, *Ind. Eng. Chem. Res.*, 2008, **47**, 9127; (*b*) W. Y. Shi, S. He, M. Wei, D. G. Evans and X. Duan, *Adv. Funct. Mater.*, 2010, **20**, 3856.

13 W. Y. Shi, M. Wei, D. G. Evans and X. Duan, *J. Mater. Chem.*, 2010, **20**, 3901.

14 (*a*) Z. P. Liu, R. Z. Ma, M. Osada, N. Iyi, Y. Ebina, K. Takada and T. Sasaki, *J. Am. Chem. Soc.*, 2006, **128**, 4872; (*b*) J. B. Han, D. P. Yan, W. Y. Shi, J. Ma, H. Yan, M. Wei, G. D. Evans and X. Duan, *J. Phys. Chem. B*, 2010, **114**, 5678.

15 (*a*) J. N. Moorthy, P. Natarajan, P. Venkatakrishnan, D. H. Huang and T. J. Chow, *Org. Lett.*, 2007, **9**, 5215; (*b*) Y. Sagara, T. Mutai, I. Yoshikawa and K. Araki, *J. Am. Chem. Soc.*, 2007, **129**, 1520; (*c*) Y. Oyamada, S. Akiyama, M. Yahiro, M. Saigou, M. Shiro, H. Sasabe and C. Adachi, *Chem. Phys. Lett.*, 2006, **421**, 295.

16 H. Zhang, Y. Wang, K. Shao, Y. Liu, S. Chen, W. Qiu, X. Sun, T. Qi, Y. Ma, G. Yu and D. Zhu, *Chem. Commun.*, 2006, 755.

17 (*a*) M. J. Sienkowska, H. Monobe, P. Kaszynski and Y. Shimizu, *J. Mater. Chem.*, 2007, **17**, 1392; (*b*) A. Hayer, V. De Halleux, A. Koehler, A. El-Garoughy, E. W. Meijer, J. Barbera, J. Tant, J. Levin, M. Lehmann, J. Gierschner, J. Cornil and Y. H. Geerts, *J. Phys. Chem. B*, 2006, **110**, 7653.

18 (*a*) H. W. Rhee, C. R. Lee, S. H. Cho, M. R. Song, M. Cashel, H. E. Choy, Y. J. Seok and J. I. Hong, *J. Am. Chem. Soc.*, 2008, **130**, 784; (*b*) A. A. Marti, S. Jockusch, N. Stevens, J. Ju and N. J. Turro, *Acc. Chem. Res.*, 2007, **40**, 402.

19 (*a*) L. Liu, D. Zhang, G. Zhang, J. Xiang and D. Zhu, *Org. Lett.*, 2008, **10**, 2271; (*b*) H. J. Kim, S. Y. Park, S. Yoon and J. S. Kim, *Tetrahedron*, 2008, **64**, 1294; (*c*) A. B. Othman, J. W. Lee, J. S. Wu, J. S. Kim, R. Abidi, P. Thuery, J. M. Strub, A. V. Dorsselaer and J. Vicens, *J. Org. Chem.*, 2007, **72**, 7634.

20 A. Koziara, K. Turski and A. Zwierzak, *Synthesis*, 1986, **4**, 298.

21 P. P. Bontchev, S. Liu, J. L. Krumhansl and J. Voigt, *Chem. Mater.*, 2003, **15**, 3669.

22 W. T. Tak and S. C. Yoon, *KSN*, 2001, **20**, 863.

23 (*a*) M. Boiocchi, L. Fabbrizzi, M. Licchelli, D. Sacchi, M. Vazquez and C. Zampa, *Chem. Commun.*, 2003, 1812; (*b*) F. Bolletta, I. Costa, L. Fabbrizzi, M. Licchelli, M. Montalti, P. Pallavicini, L. Prodi and N. Zaccheroni, *J. Chem. Soc., Dalton Trans.*, 1999, 1381.

24 J. D. Malhotra and L. H. Chen, *J. Phys. Chem. B*, 2005, **109**, 3873.

25 E. Baumann, *J. Inorg. Nucl. Chem.*, 1974, **36**, 1827.

26 K. A. Connors, *Binding Constants – The Measurement of Molecular Complex Stability*, John Wiley & Sons, New York, 1987, chapter 4.

27 J. R. Lakowicz, *Principles of Fluorescence Spectroscopy*, Kluwer Academic/Plenum Publishers, New York, 1999, chapter 8.

